AAS PrePrint 23-490

DATA-DRIVEN MODELING FOR NAVIGATION IN CISLUNAR SPACE

Matthew Brownell[*], Mackenzie Mangette[†], Roshan Eapen[‡] and Puneet Singla[§]

The main focus of this work is to identify a time-varying model to capture the differences in model fidelity for trajectories in the cislunar orbital realm. This is motivated by a lack of analytical models available that describe the high fidelity dynamics of cislunar space. Rather than finding a global model between input and output space, subspace methods for system identification will be utilized to find a subspace over which unknown dynamics evolve. This identification method allows one to obtain a simplified model that captures dominant dynamical behavior of the system as a departure from a lower fidelity model.

INTRODUCTION

Until recently, space missions have predominantly taken place in near-Earth orbital regimes (Low Earth orbit (LEO) to Geostationary orbits (GEO)). The dominant transport mechanisms within this two-body (Earth and satellite) framework can be described very accurately using osculating orbital elements and the various dynamical phenomena also persist in a higher-fidelity model.[2,6,25] The perturbed two-body (Keplerian) framework has led to extensive modeling, various approximate solutions of increasing fidelity, and analysis of representative behaviors to investigate spacecraft motion in orbits around Earth.[2,3,6,20,27] Guidance and navigation architectures are well-established for spacecraft motions in these orbital regimes.[4,9,10,12,19,23,29,30] To get closer to the ultimate objective of setting foot on Mars, there has been an increase in interest in lunar exploration in recent years.[1,17] Consequently, the exploration of cislunar space under the framework of three bodies (Earth-Moon-spacecraft) has become increasingly prevalent as the Artemis Program, headed by the National Aeronautics and Space Administration (NASA), continues the endeavor to re-initiate crewed missions to the Moon.[1,17] However, beyond GEO (XGEO), the dynamical environment shifts, and the fundamental structure of space trajectories can be radically different. Unfortunately, the chaotic nature of generic three-body trajectories renders it difficult to develop an elegant and universally applicable navigation solution.[26]

It is often overlooked that the three-body problem represents only a subset of the broader class of multi-body dynamical problems encountered in engineering. Consequently, when transitioning

[*]Ph.D. Candidate, Department of Aerospace Engineering, Pennsylvania State University, University Park, PA-16802 Email:

[†]Graduate Student, Department of Aerospace Engineering, Pennsylvania State University, University Park, PA 16802, Email: mxm6929@psu.edu.

[‡]Assistant Professor, Department of Aerospace Engineering, The Pennsylvania State University, University Park, PA 16802

[§]Professor, AIAA Associate Fellow, AAS Fellow, Department of Aerospace Engineering, The Pennsylvania State University, University Park, PA 16802

to higher-fidelity models involving more than three bodies, the dynamical structures either cease to exist or only exist in a qualitative manner requiring researchers to resort to numerical techniques.[21] Furthermore, even in low-fidelity models, global dynamical behavior has largely remained qualitative and computational, limiting the theory or nonlinear prediction, estimation, and control away from periodic orbits and fixed points,[7,8,11,13,15] such as in the case of transfers between the Earth and the Moon or between families of periodic orbits. This work is a step towards developing a framework to capture the dynamical information between two frameworks of varying fidelity, the circular restricted three-body framework and the Ephemeris framework consisting of four bodies (Sun, Earth, Moon, and spacecraft) with the position of the three more massive bodies provided by the JPL Ephemeris data.[22] The guiding principles of this work are rooted in system identification, or methods of understanding and analyzing complex systems by identifying the dynamics through discrete system matrices. The aim of this work is to provide data-driven, actionable recommendations for trajectory design in higher-fidelity space environments by identifying the dynamical model that captures differences between the two models. Specifically, the case of a transfer between a L_2 halo orbit and a L_1 Halo orbit is examined.

Utilizing inertial measurements of a spacecraft as an output of a dynamical system, previous work proposed utilizing a system identification tool– the Eigensystem Realization Algorithm (ERA)– to find the subspace over which the dynamics can be explained while approximating the input-output data with a linear, time-varying system.[?] There have also been explorations of the CR3BP from a data-driven standpoint using the Koopman operator theoretic approach.[14,18,24,28] Koopman operators essentially determine a higher-dimensional subspace where the dynamics of a dynamical system is linear.[5] However, to capture the complete dynamics of a nonlinear system, the dimension of the higher-dimensional phase-space can become infinite. Utilizing the Koopman operator-theoretic approach with system identification methods such as the ERA and dynamic mode decomposition (DMD) has enabled the discovery of intrinsic coordinates for a large number of dynamical systems, however a closure of the Koopman methods has yet not been found.[5] However, its applications to the three-body problem framework is only explored minimally.

The current work seeks to utilize this approach to quantify the differences in dynamical behavior between two model frameworks via the identification of a departure motion dynamical system. Based on these efforts, this paper offers two contributions: (i) a data-driven procedure for identifying departure dynamics along a transfer trajectory designined in a lower-fidelity model, and (ii) a demonstration of this procedure in the context of a variety of natural motions throughout the Earth–Moon neighborhood. In addition, this paper will cover the motivation, methodology, and goals of the research work. The first section following this introduction will discuss the two dynamical models in detail. Next, the problem statement is defined and the tools and algorithms used to accomplish the intended tasks will be discussed. Lastly, results will be presented and analyzed in the scope of relevant applications.

PROBLEM STATEMENT AND RELEVANT BACKGROUND

Consider a spacecraft on a transfer trajectory between the L_2 Halo orbit and an L_1 Halo orbit. The energy levels of the two Halo orbits are different. The trajectory is constructed using a shooting method employed in the Circular Restricted Three-Body Problem (CR3BP) framework.[26] Under the higher-fidelity framework i.e. the Ephemeris model, these trajectories deviate from their nominal path.[21] A core idea of this paper is to capture this deviation as a linear time-varying model using system identification methods.

The two models utilized in this study are of varying complexity with lower-fidelity three-body framework with simplifying assumptions on the motion of the two larger bodies, and four-body dynamics with the instantaneous position of the planets obtained from the JPL ephemeris for a specific epoch. There are dynamical structures that exist in the CR3BP that can be leveraged to plan transfers in the CR3BP framework. While these structures persist in the higher fidelity framework, that may not exist using the same initial conditions; understanding the *difference* between these models is an important challenge that will aid in quantifying the force-model structure differences between two dynamical models. This is the overall insight that this work seeks to obtain. System identification, specifically TVERA, allows one to quantify how the addition of one massive body (or other influential forces) affects the dynamics of a spacecraft's trajectory.

The goal is to model the perturbation from the nominal trajectory defined in the CR3BP utilizing training data produced by perturbing the spacecraft in the ephemeris model. The nominal trajectory investigated in this work is a transfer from periodic orbits about the CR3BP equilibrium points L_2 to L_1. Previous work[?] has looked at the complicated dynamics near a stable Halo orbit about L_1. The transfer between equilibrium points and the motions near the Moon dramatically changes the previously identified dynamics. The identified model is no longer valid for the dynamics found locally about an equilibrium point; instead it is locally about the transfer itself. Thus, the training data (generated using the higher-fidelity model) used will be trajectories perturbed from the transfer, which will serve as the nominal trajectory. To stress-test this system identification method, it is best to train the model with a trajectory that traverses across regions with vastly different dynamics.

The following section describes the two dynamical models used in this work.

Circular Restricted Three-Body Problem Framework

The Circular Restricted Three-Body Problem (CR3BP) model describes the motion of an object under the mutual gravitational effect of two larger masses (called primaries). The two primaries rotate about their common barycenter in a circular orbit within their orbital plane. The $\hat{x}$-axis is directed from the barycenter to the less massive primary and the $\hat{z}$-axis is in the direction of the angular momentum vector of the two primaries. Non-dimensionalization brings about a unit-eliminating simplifications in which the angular velocity of the rotating frame is $\omega = 1$ and is purely about the z direction. In addition, the time period of the primaries orbiting about their barycenter is 2π. Denoting $\mu = \frac{m_2}{m_1+m_2}$ as the mass parameter. The more massive primary, with mass m_1, is located at $(-\mu, 0, 0)$ and the other, with mass m_2, at $(1-\mu, 0, 0)$. The set up of this three-body problem is shown in Figure 1.

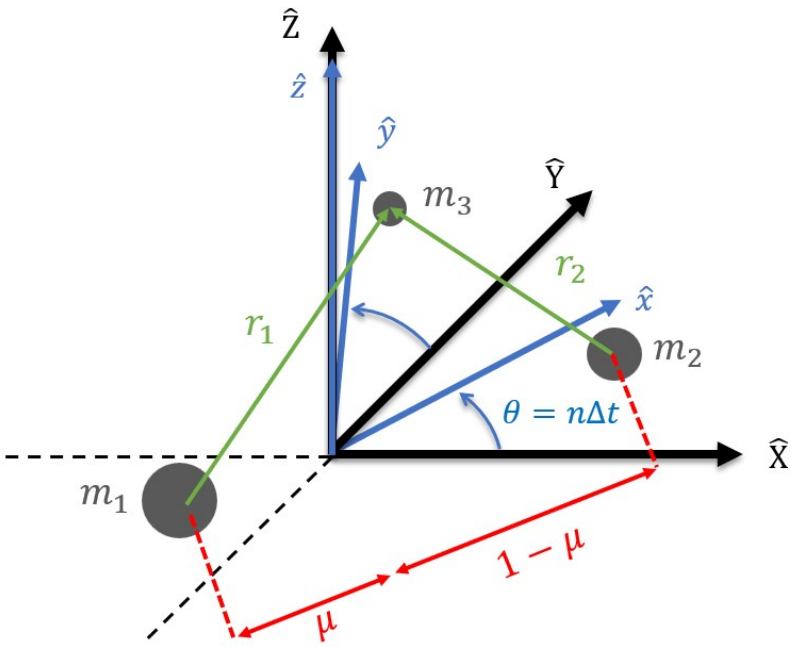

Figure 1: The Circular Restricted Three-Body Problem (CR3BP) with the Earth and Moon as the two primaries and a spacecraft as the third body of negligible mass.

The equations of motion for the CR3BP in the rotating frame can be written in vector form as shown in Eq. (1).

$$\ddot{\mathbf{q}} + 2\boldsymbol{\omega} \times \dot{\mathbf{q}} = \frac{\partial \Omega}{\partial \mathbf{q}} \tag{1}$$

where, $\boldsymbol{\omega} = [0, 0, 1]^T$ and $\mathbf{q} = [x, y, z]^T$. $\Omega = \frac{1}{2}(x^2 + y^2) + \frac{1-\mu}{r_1} + \frac{\mu}{r_2}$ is the CR3BP (CR3BP) pseudo-potential obtained by augmenting the inertial potential with the potential of the rotating frame. Lastly, $r_1 = ((x + \mu)^2 + y^2 + z^2)^{1/2}$ and $r_2 = ((x - 1 + \mu)^2 + y^2 + z^2)^{1/2}$ locate the third body with respect to the first and second primary, respectively.

The autonomous and conservative nature of the Hamiltonian H admits an integral of motion deemed the Jacobi constant, defined as $C = -2H = -|\dot{\mathbf{q}}|^2 + 2\Omega$ which is commonly used as a energy-like quantity in the CR3BP. Eq. (1) admits five equilibrium points: the so-called collinear (L_1,L_2,L_3) and triangular (L_4,L_5) points based on its location in the rotating frame.[?] The triangular points are linearly stable for a mass parameter μ less than a critical value (μ_c = 0.0385) and the collinear points are always linearly unstable. The CR3BP encompasses rich dynamical and highly nonlinear behavior, specifically in the vicinity of the equilibrium points. Next, the dynamica equationsof m otion using the JPL Ephemeris is described.

Ephemeris Model

The ephemeris model is a high-fidelity model capable of simulating finite N-body problems, such as discrete perturbations of trajectories in the solar system. These simulations are done through the MATLAB-equivalent of the SPICE tool, MICE. Specifically, the ephemeris model built for the current work will incorporate the effects of the Earth, the Moon, and the Sun expressed in the J2000 frame. It is important to note that the ephemeris model requires the formation of equations of motion

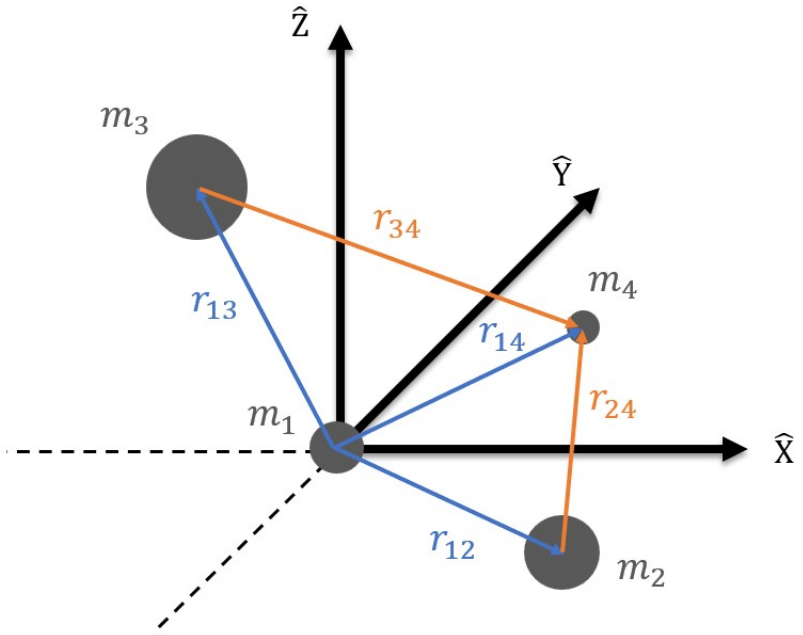

Figure 2: The four-body problem centered about m_1 where m_4 is a spacecraft of arbitrary mass.

for the body of negligible mass for propagating. The database available along with SPICE offers discrete data of the state variables (in 6 dimensions) of each of the three bodies at a given epoch. In addition, previous mission data is also available to reproduce simulations of past NASA missions. The following expression shows the equations of motion for this four-body problem:

$$\ddot{\boldsymbol{x}} = -\frac{Gm_1}{r_{14}^3} - Gm_2\left(\frac{\boldsymbol{r}_{24}}{r_{24}^3} + \frac{\boldsymbol{r}_{12}}{r_{12}^3}\right) - Gm_3\left(\frac{\boldsymbol{r}_{34}}{r_{34}^3} + \frac{\boldsymbol{r}_{13}}{r_{13}^3}\right) \tag{2}$$

G is the universal gravitational constant. $\boldsymbol{r}_{ij}$ indicates the vector from Body i to Body j, and this notation holds true through the equations of motion above. m_1 is the central body while m_4 is the spacecraft. When defining transfers in the lunar vicinity, the central body is the Moon. The set up of this four-body problem is shown in Figure 2. Due to the perturbation of three primaries on the fourth body of negligible mass, the dynamics of this body is considerably nonlinear. Ephemeris data in this work will be used in the production of training data for the identification of time-varying systems. The three-body and four-body dynamical systems can be used in conjunction to further knowledge regarding the difference in dynamics when adding another primary body.

In order to propagate, and visualize the trajectories in the two models, appropriate frame conversions are required between the osculating CR3BP frame and the J2000 frame. These conversions are described below.

Frame Transformations

To quantify the difference between the two models, one must know the transformation between them. This transformation from CR3BP to the Moon-centered J2000 frame involves the transformation of the CR3BP to the Moon-centered inertial frame. In order to identify such a transformation, an instantaneous transformation matrix is constructed. The x-axis is defined as the unit vector originating at the Earth-Moon barycenter and in the direction of the moon. The z-axis is defined in the

direction of the angular momentum of the Moon's motion. In order to find the origin of the frame, or where the Moon is in the J2000 frame, a set of ephemerides specified for the dates of propagation is used. If $\boldsymbol{r}_{CR3BP}$ is the position of the spacecraft in the CR3BP with respect to the Moon and $\dot{\boldsymbol{r}}_{CR3BP}$ is the velocity, then the transformation is performed as shown below:

$$\hat{\boldsymbol{i}}_r = \frac{\boldsymbol{r}}{||\boldsymbol{r}||} \qquad \hat{\boldsymbol{i}}_h = \frac{\boldsymbol{h}}{||\boldsymbol{h}||} \qquad \hat{\boldsymbol{i}}_r = \hat{\boldsymbol{i}}_r \times \hat{\boldsymbol{i}}_h$$

$$\boldsymbol{r}_{J2000} = \begin{bmatrix} \hat{\boldsymbol{i}}_r & \hat{\boldsymbol{i}}_y & \hat{\boldsymbol{i}}_h \end{bmatrix} \boldsymbol{r}_{CR3BP} \tag{3}$$

$$\dot{\boldsymbol{r}}_{J2000} = \begin{bmatrix} \omega\hat{\boldsymbol{i}}_y & -\omega\hat{\boldsymbol{i}}_r & \boldsymbol{0} & \hat{\boldsymbol{i}}_r & \hat{\boldsymbol{i}}_y & \hat{\boldsymbol{i}}_h \end{bmatrix} \begin{bmatrix} \boldsymbol{r}_{CR3BP} \\ \dot{\boldsymbol{r}}_{CR3BP} \end{bmatrix} \tag{4}$$

where $\omega = 2\pi/T$ and T is the period of the Moon about the Earth. The transformation from the J2000 frame to the CR3BP is done by reversing the process and transposing the matrices. Having exained the two dynamical models, the formulation of the data-driven framework used in this work is described next.

Setting-up the data-driven approach

In order to set-up the data-driven approach taken in this paper, the trajectories in the CR3BP and the Ephemeris models are compared. The general framework is as follows:

Let the equations of motion for the CR3BP be written more generally as,

$$\dot{\boldsymbol{x}} = \boldsymbol{f}(\boldsymbol{x}) \tag{5}$$

where $\boldsymbol{x} = [x, y, z, \dot{x}, \dot{y}, \dot{z}]^T$ in the rotating reference frame of the CR3BP. Consider the nominal trajectory propagated in the ephemeris model, denoted by $\boldsymbol{x}_{Nom}(t)$. If the true motion of the spacecraft is given by $\boldsymbol{x}(t)$, then the true perturbation from the nominal is

$$\delta\boldsymbol{x} = \boldsymbol{x}(t) - \boldsymbol{x}_{Nom}(t). \tag{6}$$

To learn the how the motion of the spacecraft changes as a result of integration in ephemeris model, written generally as $\dot{\boldsymbol{x}} = g(\boldsymbol{x})$, from the CR3BP, the perturbed motion is determined as follows:

$$\delta\tilde{\boldsymbol{x}} = \boldsymbol{x}_{Eph} + \delta\boldsymbol{x} - \boldsymbol{x}_{CR3BP} \tag{7}$$

$\delta\boldsymbol{x}$ is applied and tracked in the ephemeris model as the true perturbed motion of the spacecraft. This is what will be used within TVERA to learn the perturbation dynamics of the ephemeris model from the CR3BP. This learned system will be in the form of Eq. (26). Additionally, one can perform a first-order Taylor Series expansion of Eq. (5) about the same nominal trajectory to obtain an approximation of the perturbation dynamics within the CR3BP,

$$\dot{\delta\tilde{\boldsymbol{x}}} = A(x)\delta\tilde{\boldsymbol{x}} \tag{8}$$

$$A(\boldsymbol{x}) = \left.\frac{\partial \boldsymbol{f}}{\partial \boldsymbol{x}}\right|_{Nom} \tag{9}$$

This system can be discretized as,

$$\delta\tilde{\boldsymbol{x}}_{k+1} = \Phi(k+1, k)\delta\tilde{\boldsymbol{x}} = A_k\delta\tilde{\boldsymbol{x}}. \tag{10}$$

Here, $\delta\tilde{\boldsymbol{x}}$ represents the perturbation dynamics from $\boldsymbol{x}_{Nom}(t)$ when only considering the dynamics of the CR3BP. This is very different from the identified system matrix obtained via ephemeris perturbation data. The eigenvalue comparison of the system matrix defined in Eq. (10) with the identified system matrix will be of interest in the results section.

After performing TVERA/IC, the following system will be identified:

$$\delta\boldsymbol{z}_{k+1} = \hat{A}_k \delta\boldsymbol{z}_k \tag{11}$$

$$\delta\boldsymbol{x}_k = \hat{C}_k \delta\boldsymbol{z}_k \tag{12}$$

where $\hat{A}_k$ is the identified system matrix, $\hat{C}_k$ is the identified output matrix, $\delta\boldsymbol{z}_k$ is the perturbation of the identified coordinate system, which holds no *physical* meaning, and $\delta\tilde{\boldsymbol{x}}$ is the estimated departure motion in the true coordinate system. Once a system is identified, the perturbation dynamics can be used to reconstruct the nominal trajectory in the ephemeris model during the same times at which the original trajectory was propagated. The ability of the identified model to accurately reconstruct this transfer trajectory will be assessed in the presentation of results.

SYSTEM IDENTIFICATION PRELIMINARIES AND METHODOLOGY

Methodology in system identification focuses on the linearization of time-invariant or time-varying systems. For time invariant systems, a state-space representation is written as,

$$\boldsymbol{z}_{k+1} = A\boldsymbol{z}_k + B\boldsymbol{u}_k, \tag{13}$$

$$\boldsymbol{y}_k = C\boldsymbol{z}_k + D\boldsymbol{u}_k. \tag{14}$$

The linearization is not an exact model for the system; however, it provides a good approximation and interpretation of the effects of control on the system. For a more complicated dynamical system, a time-invariant system may not provide the best approximation. Thus, one can create a state-space representation in which matrices A, B, C and D are time-varying:

$$\boldsymbol{z}_{k+1} = A_k\boldsymbol{z}_k + B_k\boldsymbol{u}_k \tag{15}$$

$$\boldsymbol{y}_k = C_k\boldsymbol{z}_k + D_k\boldsymbol{u}_k \tag{16}$$

This time-varying identification process has the capability to provide a better approximation for nonlinear systems.

In the case of the CR3BP, the dynamics of the third-body are highly nonlinear, especially those that trek near the Moon. Thus, a time-varying system identification campaign will be done in order to identify the perturbation dynamics of the third body relative to a nominal trajectory. In order best identify the dynamics of the system, the third-body, or satellite of negligible mass, will not make any self-produced maneuvers during the identification process. Therefore, the control $\boldsymbol{u}_k$ will be zero. This creates an estimated representation that quantifies the initial condition response of the system, thus eliminating control values from the identified system:

$$\boldsymbol{z}_{k+1} = A_k\boldsymbol{z}_k \tag{17}$$

$$\boldsymbol{y}_k = C_k\boldsymbol{z}_k \tag{18}$$

The specific tools of system identification used in this work will be discussed in this section.

Time-Varying Eigensystem Realization Algorithm (TVERA)

The Eigensystem Realization Algorithm (ERA) is traditionally used for identifying time-invariant discrete-time systems.[16] ERA utilizes system Markov parameters, which are also invariant, in order to find the system matrices A, B, C, and D using experimental input-output data. For the time-varying case, the Time-Varying Eigensystem Realization Algorithm (TVERA) allows for the identification of a time-varying discrete-time system model. The traditional algorithm is presented utilizing generalized Markov parameters calculated using Observer/Kalman Filter Identification (OKID);[?] however, due to the zero-input nature of the experimental data presented for identification, the following algorithm is modified to suit the current problem.

For this system in which only A_k and C_k are developed for a system identified with zero-input training data, the concept of observability still applies. The observability matrix $O^{(p)}$ can be used to determine the system as observable to order n if the $pm \times n$ block of $O^{(p)}$ has a rank of n.[?] The observability matrix is set up as follows,

$$O_k^{(p)} = \begin{bmatrix} C_k \\ C_{k+1}A_k \\ C_{k+2}A_{k+1}A_k \\ \cdots \\ C_{k+p-1}A_{k+p-2}...A_0. \end{bmatrix} \tag{19}$$

where p indicates the order of the observer. The Hankel matrix will not be built using generalized or system Markov parameters as shown in traditional ERA and TVERA; instead, it will be filled with output data from N experiments. The Hankel matrix can be set up as follows:[?]

$$\tilde{H}_k^{p,N} = \begin{bmatrix} y_k^{\#1} & y_k^{\#2} & \cdots & y_k^{\#N} \\ y_{k+1}^{\#1} & y_{k+1}^{\#2} & \cdots & y_{k+1}^{\#N} \\ \vdots & \vdots & \ddots & \vdots \\ y_{k+p-1}^{\#1} & y_{k+p-1}^{\#2} & \cdots & y_{k+p-1}^{\#N} \end{bmatrix} \tag{20}$$

The training data for each experiment will be used up to the $(k + p - 1)$ time step in order to sufficiently fill out the Hankel matrix. Note the parameters p and N are chosen by the user to capture order n of the system. Using the modified Hankel matrix, one can continue with the familiar approach of obtaining the minimum realization by taking the singular value decomposition (SVD) of $\tilde{H}_k$, which will isolate values similar to eigenvalues for an overdetermined system.

$$\begin{aligned} \tilde{H}_k &= O_k^{(p)} X_k^{(N)} = U_k \Sigma_k^{1/2} \Sigma_k^{1/2} V_k^T \\ &= \begin{bmatrix} U_k^{(n)} & U_k^{(0)} \end{bmatrix} \begin{bmatrix} \Sigma_k^{(n)} & 0 \\ 0 & \Sigma_k^{(0)} \end{bmatrix} \begin{bmatrix} V_k^{(n)^T} \\ V_k^{(0)^T} \end{bmatrix} \\ &\approx U_k^{(n)} \Sigma) k^{1/2} \Sigma_k^{1/2} V_k^{(n)^T} \end{aligned} \tag{21}$$

Thus, the minimum realization of the identified discrete-time time-varying system is,

$$\hat{A}_k = \Sigma_{k+1}^{n^{1/2}} V_{k+1}^{(n)^T} V_k^{(n)} \Sigma_k^{n^{-1/2}} \tag{22}$$

$$\hat{C}_k = E^{(m)^T} U_k^{(n)} \Sigma_{k+1}^{n^{1/2}} \tag{23}$$

$$\hat{X}_0 = \Sigma_0^{n^{-1/2}} U_0^{(n)^T} \tilde{H}_0. \tag{24}$$

Note m is the number of outputs or the length of y_k and $E^{(m)^T} = \begin{bmatrix} I_m & O_m & \dots & O_m \end{bmatrix}$. This SVD is performed at each time step of interest and yields the state-space model,

$$\boldsymbol{z}_{k+1} = A_k \boldsymbol{z}_k \tag{25}$$

$$\boldsymbol{y}_k = C_k \boldsymbol{z}_k. \tag{26}$$

The identified state $\mathbf{z}$ may not have the same dimension as the original state and has no physical meaning. The output y is the same output as the reference system.

Similarity Transformations

A time-varying transformation between one coordinate systems is written generally as,

$$\boldsymbol{z}_k = T_k \boldsymbol{x}_k, \tag{27}$$

where, in our case, $\boldsymbol{z}$ is the identified state vector obtained using TVERA and $\boldsymbol{x}$ is the reference state (position and velocity for this paper). The identified system's state-space can be reqritten as,

$$\boldsymbol{z}_{k+1} = T_{k+1}^{-1} A_k T_k \boldsymbol{z}_k \tag{28}$$

$$= \hat{A}_k \boldsymbol{z}_k. \tag{29}$$

Unlike in time-invariant systems, $\hat{A}_k$ is not a similarity transformation of A_k. Instead, it is a more general topological transformation. A_k and $\hat{A}_k$ do not have the same eigenvalues at any time k. This also implies that the system evolution takes place in different coordinates systems, T_k and T_{k+1}. However, the ability to compare the eigenvalues of both matrices enhances the analysis and evaluation of the final estimated model. Thus, A_k and $\hat{A}_k$ must undergo linearization transformations,

$$\begin{aligned}
\tilde{\hat{A}}_k &= O_k^\dagger O_{k+1} \hat{A}_k \\
&= T_k^{-1} O_k^\dagger O_{k+1} T_{k+1} T_{k+1}^{-1} A_k T_k \\
&= T_k^{-1} O_k^\dagger O_k^\dagger O_{k+1} A_k T_k \\
&= T_k^{-1} \tilde{A}_k T_k.
\end{aligned}$$

As a result of this transformation, the system matrices $\tilde{A}_k$ and $\tilde{\hat{A}}_k$ are now similarity transformations of one another and their eigenvalues can be compared at each time step. The linearity of the system defines if the true and identified eigenvalues match. In the case of the dynamical system estimated in this work, the true system is nonlinear; therefore, the eigenvalues are not expected to match.

APPLICATION TO TRANSFER TRAJECTORIES IN THE CR3BP

In this paper, the purpose of TVERA is to identify the perturbation dynamics that result from forces besides the Earth and Moon when in cislunar space. To do this, perturbation data must be obtained relative to a nominal trajectory within the CR3BP. Given the lack of experimental data available, this perturbation data must be manufactured via an Ephemeris model. Once a nominal trajectory within the CR3BP is defined, a set of 'near-by' trajectories are propagated in the Ephemeris model and serve as the 'training' trajectories. The nominal trajectory transformed to the appropriate

frame is then subtracted from these training trajectories to obtain the perturbation data set. This data is utilized within TVERA to obtain a state-space model for the perturbation dynamics from the CR3BP. In essence, the training trajectories define the subspace, or figuratively the 'tube', that TVERA is identifying with a linear, time-varying model.

The training trajectories are chosen to be transfers from a Halo orbit about L_2 to another Halo orbit about L_1 in the CR3BP. This set of transfer trajectories is shown in Figure 3(a). The process of manufacturing the perturbation data is summarized as follows:

1. A set of 10 initial and 10 final states on both the starting L_2 Halo and final L_1 Halo are chosen arbitrarily. These 10 states on each Halo are evenly spaced in time from each other.

2. Transfers are calculated for every combination of initial and final state within the CR3BP via an impulsive velocity change. This results in 100 transfer trajectories. The nominal orbit is then chosen to be the transfer trajectory between the 5^{th} initial state and 5^{th} final state (i.e. the 'middle' trajectory is the nominal). This leaves 99 transfer trajectories for data acquisition.

3. Propagate all 99 transfer trajectories' initial states within the ephemeris model. This paper assumes measurements of position and velocity of the spacecraft are obtained every 5 minutes.

4. Obtain perturbation data by subtracting the nominal trajectory from the ephemeris trajectories found in the previous step

The CR3BP reference trajectories, the ephemeris trajectories, and the ephemeris perturbations are all shown in Figure 3. Note that all states are converted back to the CR3BP rotating reference frame.

After obtaining the identified state-space model with the perturbation data, the estimated output is compared to the reference ephemeris perturbations. The following methodology is implemented to achieve this:

1. Randomly choose 30 of the 99 transfer trajectories as the training data set to learn the identified model with.

2. Use the other 69 trajectories as the 'experimental' data set to test the validity of the identified system. Observe average replication error over time.

The average replication error across the experimental data set is shown in Figure 4 along with the singular value plot (SVP) from the singular value decomposition within TVERA. Within the SVP, there are 6 dominant singular values over time as expected, as this is the number of states in real coordinate space; however, there are a few non-dominant singular values that are of unexpected magnitudes. This most likely occurs due to the original system being highly nonlinear in nature. The average output replication is low but increases over propagation time. From first glance, TVERA is successfully able to capture the perturbation dynamics for the given set of trajectories.

Additionally, it is of interest to observe how the eigenvalues of the nominal trajectory's system matrix compare to that of the identified system matrix. This corresponds to the system matrices in equations (10) and (11), respectively. This comparison is shown in Figure 5. The blue circles are the nominal system matrix's eigenvalues, the green markers indicate the identified system matrix's eigenvalues, and the black line is the unit circle. Clearly, the identified eigenvalues do not match the nominal. They are both localized to the same area of the unit circle, but have extremely different

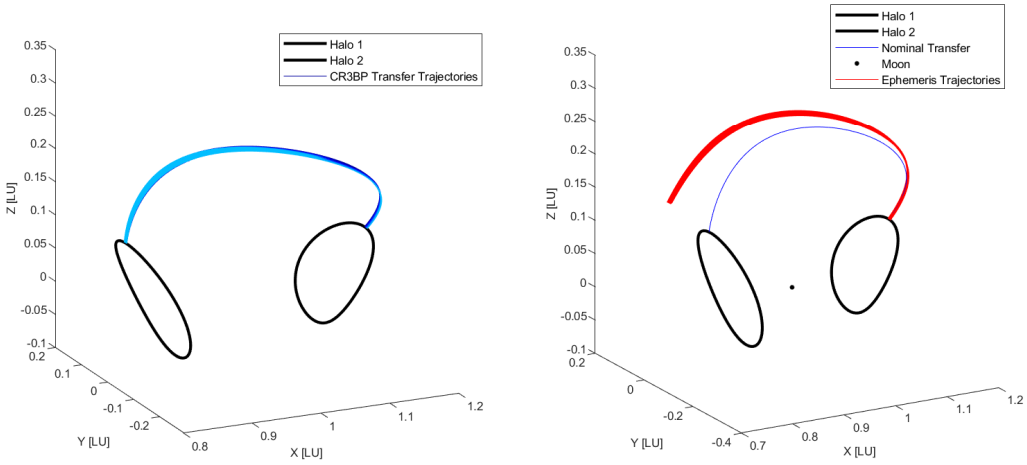

(a) CR3BP (b) Ephemeris

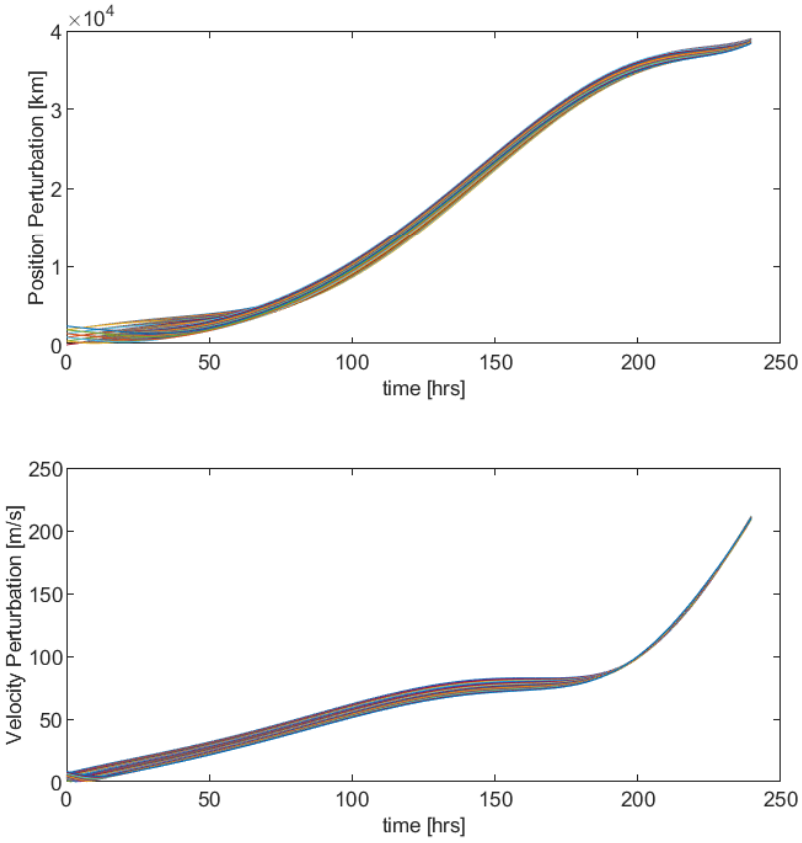

(c) Ephemeris Trajectories' perturbations over time

Figure 3: Transfer trajectories propagated in CR3BP and ephemeris

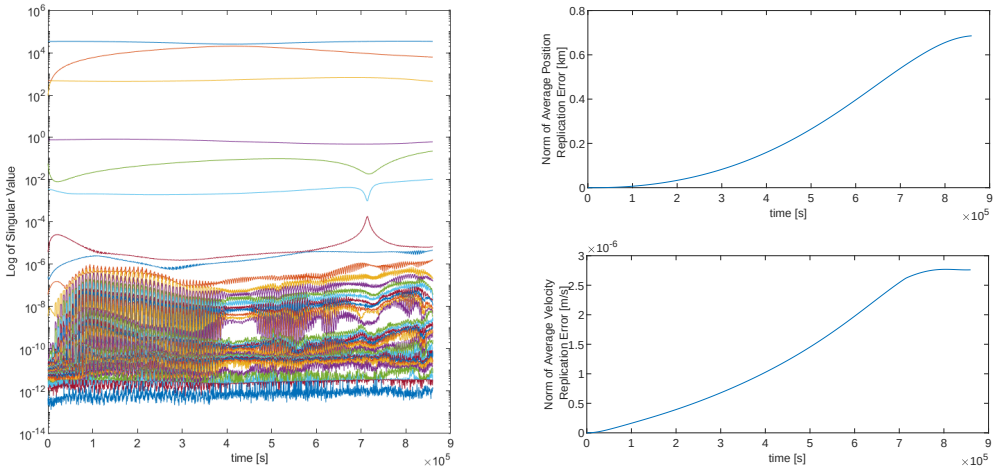

(a) Singular Value Plot

(b) Average Output Replication Error

Figure 4: Identified System's singular value plot and replication error

shapes. The identified eigenvalues also seem to diverge outside the unit circle over time. Note that Figure 5 displays the eigenvalues post transformation defined in the *Similarity Transformations* Section.

Recalling the 'tube' the training trajectories define, a case study is performed to observe how the size of this tube affects the validity of the identified model. The size of the tube is increased by spacing out the 10 initial and final conditions more and decreased by spacing them out less. The data shown previously has the states on each Halo orbit spaced out by approximately 2300 km, but varies slightly between states since the velocity is not constant on these orbits. By spacing out the initial and final states more, the resultant training trajectories span spaces further apart from each other. This results in TVERA attempting to cast a large amount of propagation data with nonlinear dynamical behavior into a linear, time-varying system. Intuitively, it is expected that the identified model will perform worse in this case with fewer discrete samples. Conversely, crowding the states further together is expected to decrease the tube and therefore decrease the replication error of the identified model. Table 1 confirms this expectation. To obtain the percent errors in Table 1, TVERA is performed 10 times with the 30 training transfer trajectories being selected randomly each time. The percent error of the identified system's output is then averaged over three things: the 10 system identification campaigns, the 69 experimental trajectories, and time.

Additionally, Table 2 presents a case study for how the chosen order of the identified system affects output replication. It is known that the true dynamics have a six degree-of-freedom state space, but the SVP shown in Figure 5(a) does not have 6 clearly distinct singular values. Table 2 displays the trend of increasing model order decreasing the replication error. It is expected that adding more dimension to the identified system will decrease the replication error; however, it is unexpected that the 8^{th} order system has a substantial decrease in replication error compared to the 6^{th} order system. The decrease in replication error with higher-order systems is due to the attempts to quantify highly nonlinear effects in the region chosen for identification by capturing these dynamics in more states with no physical meaning.

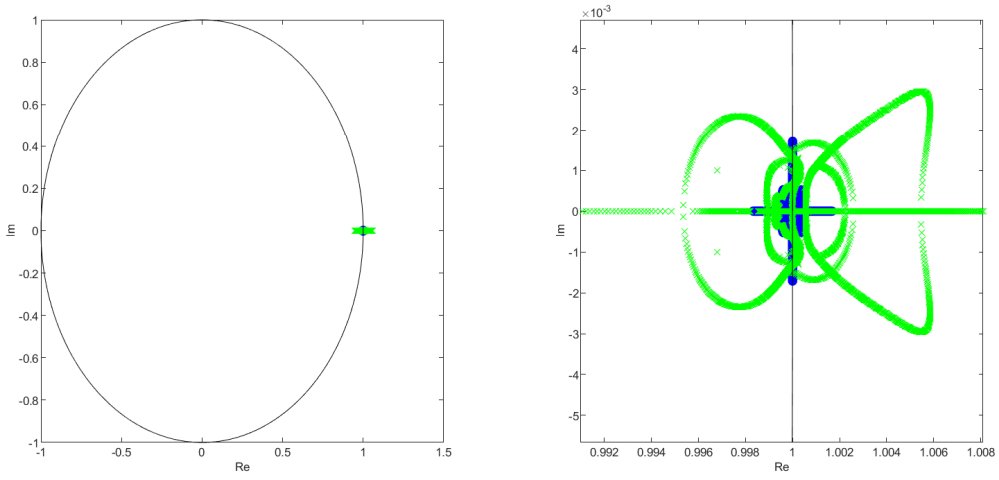

(a) Full View of Unit Circle

(b) Zoomed View

Figure 5: Comparison of Eigenvalues of Reference Trajectory and Identified System Matrix

Orbit IC Spacing (km)	Average Percent Error in Position	Average Percent Error in Velocity
≈ 25489	4.22%	15.96%
≈ 4797	1.59%	3.16%
≈ 2376	1.21%	1.92%
≈ 470	0.21%	0.31%
≈ 235	0.09%	0.13%

Table 1: Case study on how training data size affects average output replication. Lower percentage error indicates that the model has sufficiently replicated the dynamics.

Identified Model Order	Average Percent Error in Position	Average Percent Error in Velocity
2	140.78%	146.79%
4	13.17%	12.85%
6	0.79%	1.27%
8	0.08%	0.12%
10	0.08%	0.11%

Table 2: Case study on how identified model order affects average output replication. Lower percentage error indicates that the model has sufficiently replicated the dynamics.

As TVERA is a data-driven modeling method, the quality and quantity of data has immense impact on the validity of the identified model. There are many other case studies that can be performed including, but not limited to: sensor noise, number of training trajectories used, and different types of trajectories within the CR3BP. Another impact regarding the ephemeris model is the dates during which the trajectory is propagated, as this affects the positions and motion of the primaries in the four-body problem. For an analyst using the identified model on a real system, these are all important things to keep in mind.

CONCLUSION

Identifying a model that quantifies and linearizes the effects of more primaries on a spacecraft is successfully and efficiently captured utilizing TVERA. The identification of a linear time-varying model, especially with higher orders, allows one to replicate the complicated nonlinear dynamics that result from multiple primaries' gravitational pull. The model's replication process is also quick and of little computational burden. As seen through the test cases, training the model more on the front end can improve its replication capabilities and provide a more accurate approximation for the true perturbed dynamics. This also gives an intuitive reference to the growth of perturbations over time due to fourth-body effects, such as the Sun in the Earth-Moon-Sun four-body problem.

The model presented in this paper has shown the effectiveness of using TVERA to identify a linear time-varying system with initial condition response. System identification methods allow for one to extend this model to include transient response. Thus, the identification of perturbation dynamical models can be utilized to design strategies and employing station-keeping about the nominal trajectory. The success of this model with identifying the pure perturbed dynamical behavior of a spacecraft in many-body problems sheds light on the potentiality of this work's extension to utilizing model for decision-making in the mission design process.

ACKNOWLEDGEMENT

This material is based upon work supported jointly by the AFOSR grants FA8550-20-10176 and FA9550-22-1-0092.

REFERENCES

[1] Vassilis Angelopoulos. The artemis mission. *The ARTEMIS mission*, pages 3–25, 2014.

[2] Richard H Battin. *An introduction to the mathematics and methods of astrodynamics*. Aiaa, 1999.

[3] Giulio Baù, Claudio Bombardelli, and Jesús Peláez. A new set of integrals of motion to propagate the perturbed two-body problem. *Celestial Mechanics and Dynamical Astronomy*, 116(1):53–78, 2013.

[4] Giulio Baù, Claudio Bombardelli, Jesús Peláez, and Enrico Lorenzini. Non-singular orbital elements for special perturbations in the two-body problem. *Monthly Notices of the Royal Astronomical Society*, 454(3):2890–2908, 2015.

[5] Steven L Brunton and J Nathan Kutz. *Data-driven science and engineering: Machine learning, dynamical systems, and control*. Cambridge University Press, 2019.

[6] Claude Alain Burdet. Theory of kepler motion: the general perturbed two body problem. *Zeitschrift für angewandte Mathematik und Physik ZAMP*, 19(2):345–368, 1968.

[7] Maciej J Capiński and Pablo Roldán. Existence of a center manifold in a practical domain around l_1 in the restricted three-body problem. *SIAM Journal on Applied Dynamical Systems*, 11(1):285–318, 2012.

[8] Alessandra Cellett and Laura Ferrara. An application of the nekhoroshev theorem to the restricted three-body problem. *Celestial Mechanics and Dynamical Astronomy*, 64:261–272, 1996.

[9] John A Christian and Courtney L Hollenberg. Initial orbit determination from three velocity vectors. *Journal of Guidance, Control, and Dynamics*, 42(4):894–899, 2019.

[10] Emilian-Ionuţ Croitoru and Gheorghe Oancea. Satellite tracking using norad two-line element set format. *Scientific Research and Education in the Air Force-AFASES*, 1:423–431, 2016.

[11] Jacques Féjoz. Quasiperiodic motions in the planar three-body problem. *Journal of Differential Equations*, 183(2):303–341, 2002.

[12] Kohei Fujimoto, Daniel J Scheeres, and K Terry Alfriend. Analytical nonlinear propagation of uncertainty in the two-body problem. *Journal of Guidance, Control, and Dynamics*, 35(2):497–509, 2012.

[13] Antonio Giorgilli, Amadeo Delshams, Ernest Fontich, Luigi Galgani, and Carles Simó. Effective stability for a hamiltonian system near an elliptic equilibrium point, with an application to the restricted three body problem. *Journal of differential equations*, 77(1):167–198, 1989.

[14] Yuto Hirose, Mai Bando, and Shinji Hokamoto. Spacecraft trajectory design using data-driven model predictive control. In *IAF Astrodynamics Symposium 2021 at the 72nd International Astronautical Congress, IAC 2021*. International Astronautical Federation, IAF, 2021.

[15] Angel Jorba and Jordi Villanueva. Numerical computation of normal forms around some periodic orbits of the restricted three-body problem. *Physica D: Nonlinear Phenomena*, 114(3-4):197–229, 1998.

[16] Jer-Nan Juang and Richard S Pappa. An eigensystem realization algorithm for modal parameter identification and model reduction. *Journal of guidance, control, and dynamics*, 8(5):620–627, 1985.

[17] Kathy Laurini, JC Piedboeuf, B Schade, K Matsumoto, F Spiero, and A Lorenzoni. The global exploration roadmap. *IAC-11 B*, 3, 2018.

[18] Richard Linares. Koopman operator theory applied to the motion of satellites. *Advances in the Astronautical Sciences*, 171, 2019.

[19] Yazhong Luo, Jin Zhang, and Guojin Tang. Survey of orbital dynamics and control of space rendezvous. *Chinese Journal of Aeronautics*, 27(1):1–11, 2014.

[20] Don Mittleman and Don Jezewski. An analytic solution to the classical two-body problem with drag. *Celestial mechanics*, 28:401–413, 1982.

[21] Beom Park and Kathleen C Howell. Leveraging intermediate dynamical models for transitioning from the circular restricted three-body problem to an ephemeris model. In *AAS/AIAA Astrodynamics Specialist Conference*. American Astronautical Society Charlotte, North Carolina, 2022.

[22] Ryan S Park, William M Folkner, James G Williams, and Dale H Boggs. The jpl planetary and lunar ephemerides de440 and de441. *The Astronomical Journal*, 161(3):105, 2021.

[23] Juan Félix San-Juan, Iván Pérez, Montserrat San-Martín, and Eliseo P Vergara. Hybrid sgp4 orbit propagator. *Acta Astronautica*, 137:254–260, 2017.

[24] Simone Servadio, David Arnas, and Richard Linares. Dynamics near the three-body libration points via koopman operator theory. *Journal of Guidance, Control, and Dynamics*, 45(10):1800–1814, 2022.

[25] Stefano Speretta, PP Sundaramoorthy, and EKA Gill. Long-term performance analysis of norad two-line elements for cubesats and pocketqubes. *Proceedings Small Satellites for Earth Observation*, 2017.

[26] Victor Szebehely and E Grebenikov. Theory of orbits-the restricted problem of three bodies. *Soviet Astronomy, Vol. 13, p. 364*, 13:364, 1969.

[27] Laurence G Taff. Celestial mechanics: a computational guide for the practitioner. *A Wiley-Interscience Publication*, 1985.

[28] Haoze Tang et al. Koopman reduced order control for three body problem. *Modern Mechanical Engineering*, 9(01):20, 2019.

[29] David Vallado and Paul Crawford. Sgp4 orbit determination. In *AIAA/AAS Astrodynamics Specialist Conference and Exhibit*, page 6770, 2008.

[30] David A Vallado. *Fundamentals of astrodynamics and applications*, volume 12. Springer Science & Business Media, 2001.